SLAC-PUB-16485

Thermodynamic Guiding Principles in Selective Synthesis of Strontium Iridate Ruddlesden-Popper Epitaxial Films

K. Nishio,[1,2,a)] H. Y. Hwang,[1,2] and Y. Hikita[2]

[1]*Department of Applied Physics, Geballe Laboratory for Advanced Materials, Stanford University, 476 Lomita Mall, Stanford University, Stanford, California, 94305, USA*

[2]*Stanford Institute for Materials and Energy Sciences, SLAC National Accelerator Laboratory, 2575 Sand Hill Road, Menlo Park, California, 94025, USA*

We demonstrate the selective fabrication of Ruddlesden-Popper (RP) type $SrIrO_3$, $Sr_3Ir_2O_7$, and Sr_2IrO_4 epitaxial thin films using pulsed laser deposition (PLD). The RP strontium iridate series is an ideal system for studying the concerted effects of electron correlation and spin-orbit interaction. Their unique physical properties susceptible to lattice distortions motivate studies in epitaxial thin film form. However, improvement in the film quality remains a challenge due to the noble metal character of iridium and the existence of the gaseous IrO_3 species. Here we fabricated three different RP phases from a single $SrIrO_3$ target by actively controlling the Ir/Sr ratio in the films. Through systematic growth studies, we identified that the growth conditions stabilizing each RP phase directly map onto the phase diagram expected from thermodynamic equilibria. This synthetic approach allows precise control over the cation stoichiometry as evidenced by the stabilization of single phase $Sr_3Ir_2O_7$ for the first time, overcoming the close thermodynamic stability between neighboring RP phases. Despite the non-equilibrium nature of PLD, these results highlight the importance of thermodynamic guiding principles to strategically synthesize the targeted phase in complex oxide thin films.

THE MANUSCRIPT

Iridium oxides and their derivatives have attracted considerable attention as prototypical materials for exploring the effects of large spin-orbit coupling due to the heavy Ir-element.[1-3] The perovskite iridates and its extended family of the Ruddlesden-Popper (RP) series $Sr_{n+1}Ir_nO_{3n+1}$ ($n = 1, 2, \cdots, \infty$) is a representative system, evolving from a paramagnetic metal $SrIrO_3$ ($n = \infty$),[4] to the so-called spin-orbit Mott insulators $Sr_3Ir_2O_7$ ($n = 2$)[5,6] and Sr_2IrO_4 ($n = 1$)[7-10] due to the concerted effect of strong electron correlation and spin-orbit coupling.[11] These drastic changes in their physical properties strongly depend on the number of the interleaving perovskite blocks (n) between rock-salt SrO layers. Based on these bulk properties, epitaxial thin films of $Sr_{n+1}Ir_nO_{3n+1}$ have been recognized as an ideal structure for studying the lattice distortions in well-defined crystallographic orientations while tuning the dimensionality of the system as shown in the cases of $SrIrO_3$[12, 13] and Sr_2IrO_4[14-16] thin films on various substrates. For such studies, pulsed laser deposition (PLD) is the most widely used technique for fabricating the thin films. One of the biggest challenges in the growth of iridate thin films by PLD is considered to be the control of the iridium oxidation state. The noble metal character of iridium requires

This material is based upon work supported by the U.S. Department of Energy, Office of Science, Office of Basic Energy Sciences, Division of Materials Sciences and Engineering, under Contract No. DE-AC02-76SF00515.

high oxygen chemical potential; however, at excessively oxidizing conditions, gaseous IrO_3 is generated resulting in loss of iridium from the films. [17] Although deleterious for standard stoichiometric transfer of the target materials to the substrate, [18-20] use of such gaseous metal-oxide species enables the active control of the film cation stoichiometry as reported for the case of strontium ruthenate RP phases. [21-23] In this study, we systematically reduced the film Ir/Sr ratio by controlling the thermodynamic conditions during growth, and succeeded in stabilizing three phases of $Sr_{n+1}Ir_nO_{3n+1}$ (n = 1, 2, and ∞) epitaxial thin films from a single stoichiometric $SrIrO_3$ target, including $Sr_3Ir_2O_7$ epitaxial thin films for the first time. Careful examination of the obtained growth phase diagram reveals close correspondence with bulk phase stability calculations based on chemical equilibria, suggesting the dominance of thermodynamic considerations during the non-equilibrium growth process. We believe these results will be highly relevant for many other RP compounds.

A PLD system equipped with the capability to monitor the laser intensity during growth was used in this study. [24] The KrF excimer laser (wavelength 248 nm, pulse duration ~ 20 ns) beam operated at 3 Hz was imaged at an angle of 45° to the stoichiometric polycrystalline $SrIrO_3$ target. The target-substrate distance was set to 50 mm. $Sr_{n+1}Ir_nO_{3n+1}$ (n = 1, 2, and ∞) thin films were deposited on $SrTiO_3$ (001) substrates (5 × 5 mm^2 and 0.5 mm in thickness) by varying the laser fluence F, partial oxygen pressure P_{O2}, and substrate temperature T_{sub} from 0.75 to 3.78 $J{\cdot}cm^{-2}$, from 10 to 300 mTorr, and from 600 to 1000 °C, respectively. Phase identification of the films was performed by out-of-plane X-ray diffraction (XRD) and reciprocal space mapping using a diffractometer equipped with a four-bounce Ge (220) monochromator and a Cu target (wavelength 1.5406 Å). The film resistivity was measured using the four-probe method inside a temperature controlled liquid helium cryostat.

Figure 1 presents three ca. 100 nm thick RP phases selectively fabricated in single-phase form. The crystal structures of $SrIrO_3$, $Sr_3Ir_2O_7$, and Sr_2IrO_4 on (001)-oriented $SrTiO_3$ substrates are schematically illustrated in Figure 1a. By analyzing the X-ray diffraction (XRD) patterns, we were able to unambiguously identify the phase and epitaxial relationship between the films and $SrTiO_3$ (001) substrates. As evidenced by the 00h and the $\bar{1}\bar{1}3$ diffractions in Figure 1c and 1d, the orthorhombic $SrIrO_3$ thin films are stabilized along the (001)-orientation, [25] not in the ambient pressure stable monoclinic form. [26] Here we denote this in the pseudo-cubic notation. The $Sr_3Ir_2O_7$ thin film exhibits c-axis orientation based on the conventional tetragonal lattice (space group $I4/mmm$ [27]) as seen by the series of 00l peaks in the out-of-plane diffraction and the $\bar{1}\bar{1}\underline{16}$ peak near the $\bar{1}\bar{1}3$ peak of $SrTiO_3$ in

reciprocal space mapping (RSM) in Figure 1c and 1e. We note that $Sr_3Ir_2O_7$ has recently been refined to have the orthorhombic lattice with space group *Bbcb* [28] and *Bbeb*, [29] but the lattice constant differences from the tetragonal lattice is indistinguishable from our XRD measurements. Similarly, *c*-axis orientation was observed for the K_2NiF_4-type (space group $I4_1/acd$ [30]) Sr_2IrO_4 film from the 00*l* diffraction in the out-of-plane XRD and $20\underline{1}8$ reflection in RMS shown in Figure 1c and 1f. The temperature dependent resistivity of these films shows close correspondence with those reported for bulk $SrIrO_3$, $Sr_3Ir_2O_7$, and Sr_2IrO_4 as shown in Figure 1b. [4-10]

Insight into the mechanism of selective phase evolution can be obtained from a systematic growth study varying the oxygen partial pressure P_{O2} and the substrate temperature T_{sub}. Figure S1a-e show the out-of-plane XRD patterns for the films grown in the range from T_{sub} = 600 – 1000 °C and P_{O2} = 10 – 300 mTorr while fixing the laser fluence F at 3.75 J·cm^{-2}. Under all P_{O2} studied, increase in T_{sub} led to a transformation of the $SrIrO_3$ to the Sr_2IrO_4 phase with a narrow stability window for $Sr_3Ir_2O_7$ at T_{sub} = 800 – 850 °C and P_{O2} > 50 mTorr. The out-of-plane lattice constants were calculated for each growth condition. Within the stability window for $SrIrO_3$, at T_{sub} < 800°C, its pseudo-cubic lattice constant decreases and converges with increase in T_{sub} for all P_{O2}. The converged value approaches the bulk value with reducing P_{O2}, as illustrated by the dashed line in Figure 2a. Above T_{sub} = 800°C, however, the formation of $SrIrO_3$ begins to compete with $Sr_3Ir_2O_7$ and Sr_2IrO_4 formation, crossing over from Sr_2IrO_4 to $Sr_3Ir_2O_7$ at P_{O2} = 50 mTorr with increase in P_{O2}. In the region of single phase $Sr_3Ir_2O_7$ films, the *c*-axis lattice constant was sensitive to T_{sub}, changing from 20.81 Å to 20.96 Å spanning across the bulk value of 20.879 Å [27] even by 50 °C increment in T_{sub}, as shown in Figure 2b. Under the conditions stabilizing Sr_2IrO_4, the *c*-axis lattice constant approached its bulk value (Figure 2c) with increasing T_{sub} similar to the case of $SrIrO_3$.

A summary of the growth phase diagram derived from these results is presented in Figure 3a. In order to assess the role of the suggested reaction intermediate, IrO_3, we focus on the thermodynamic aspects in the selective formation of these RP phases. First, we consider the following chemical equilibrium:

$$Sr_2IrO_4\ (s) + Ir\ (s) + O_2\ (g) = 2SrIrO_3\ (s) \quad (1).$$

The phase boundary curve for Equation 1 was calculated by using the experimentally obtained standard Gibbs energies of formation for the specific binary and ternary oxides. [17, 31] The experimental phase boundary between $SrIrO_3$ and Sr_2IrO_4 as well as the appearance of (001)-oriented iridium metal at the most reducing conditions (P_{O2} = 10 mTorr, T_{sub} ≥ 950 °C) is in excellent agreement with the prediction

from Equation 1; reducing conditions shift the equilibrium toward the left following Le Chatelier's Principle. It is noteworthy that the $Sr_3Ir_2O_7$ phase is stabilized in between the stability regions for $SrIrO_3$ and Sr_2IrO_4; co-existing with $SrIrO_3$ at T_{sub} = 700 – 800 °C, and eventually forming single-phase $Sr_3Ir_2O_7$ at higher T_{sub} and P_{O2}. An exact phase boundary calculation is limited due to the lack of thermochemical data for $Sr_3Ir_2O_7$, but instead we estimate its stability window based on two characteristic trends commonly observed in other RP series containing different cations (See Supporting Information). Firstly, oxidizing (reducing) conditions are favored for RP phases with higher (lower) *n*, due to the larger electronegativity of transition metal ions compared to the alkaline earths requiring more oxygen as the transition metal content increases (Figure S2). Secondly, the stability window shrinks for higher *n* phases, due to the decreasing difference in Gibbs free energy of formation between the neighboring RP phases. The experimentally obtained $Sr_3Ir_2O_7$ stability region as well as the high sensitivity of the *c*-axis to the growth conditions follow these two thermodynamically trends expected for RP phase stability.

At higher temperatures (T_{sub} > 850 °C), the role of IrO_3 becomes important as can be seen from the following two equilibria:

$$4SrIrO_3(s) + O_2(g) = 2Sr_2IrO_4(s) + 2IrO_3(g) \qquad (2),$$

$$2Sr_2IrO_4(s) + 2Ir(s) + 3O_2(g) = 2Sr_2IrO_4(s) + 2IrO_3(g) \qquad (3).$$

Equation 2 is the equilibrium responsible for the loss of Ir from a $SrIrO_3$ film converting into Sr_2IrO_4 at higher P_{O2}, and Equation 3 is the formation of gaseous IrO_3 from solid iridium metal. We note that the phase boundaries from Equation 2 and 3 drawn as dotted lines in Figure 3 require an additional parameter, the partial pressure of IrO_3 (P_{IrO3}), which was set to 4×10^{-6} Torr in the calculations shown in Figure 3a. Although we cannot experimentally quantify P_{IrO3}, the Sr_2IrO_4 phase was stabilized at significantly lower temperatures for a series of films grown at P_{O2} = 100 mTorr under the reduced laser fluence of 0.78 J·cm^{-2} suggesting a strong correlation between *F* and P_{IrO3} as shown in Figure 3b and Figure S1f. The calculated phase boundary in Figure 3b corresponds to a P_{IrO3} of 1×10^{-7} Torr illustrating that lower P_{IrO3} corresponds to a $SrIrO_3/Sr_2IrO_4$ phase boundary shift towards lower temperatures, shrinking the stability window for $SrIrO_3$. To confirm the direct correlation between *F* and P_{IrO3}, we further studied the evolution of the RP phases by systematically reducing *F* at P_{O2} = 100 mTorr and T_{sub} = 850 °C, resulting in the phase evolution from $Sr_3Ir_2O_7$ to Sr_2IrO_4 as detected by XRD in Figure 4a. Moreover, the reduction in *F* concomitantly reduced the ex-situ determined deposition rate, a

quantity proportional to the volume of the ablated species as shown in Figure 4b. Given the gaseous form of the ablated species, it is natural to assume that the volume of the Ir-containing species, including IrO_3, at the growth surface scales with F, effectively controlling P_{IrO3}. These two results strongly support the dominance of Equation 2 and 3 in defining the phase boundaries for stabilizing the Sr_2IrO_4 phase at high temperatures.

It is quite remarkable that close correspondence is found between the growth experiments and thermodynamic calculations, considering the non-equilibrium nature of PLD growth such as: the pulsed supply of precursors, high kinetic energy of the ablated species, etc. [32] The consistency with chemical equilibria in this study is due in part to the diffusive regime employed in the deposition, where the laser-ablated species experience multiple scattering before adsorbing on the growth surface, producing a growth environment much closer to equilibrium than the ballistic regime. Signatures attributable to kinetic effects indeed become notable as we enter increasingly non-equilibrium environments, such as the absence of a phase-pure $Sr_3Ir_2O_7$, and obscured phase boundaries between the three RP phases around T_{sub} = 700 – 750 ^{o}C and P_{O2} = 10 – 20 mTorr. These conditions correspond to lower temperatures where adatom migration is slow, and low P_{O2}.

The selective fabrication of three pure phases of $Sr_{n+1}Ir_nO_{3n+1}$ (n = 1, 2, and ∞) epitaxial thin films by PLD, from a single $SrIrO_3$ target, shows that thermodynamic considerations provide a powerful guideline even for non-equilibrium thin film growth. Furthermore, given the increasing interest in layered complex oxide thin films to explore various atomic degrees of freedom, [33, 34] the growth strategy employed in this study should be effective in fabricating a wide range of RP phases containing cations with accessible volatile oxides.

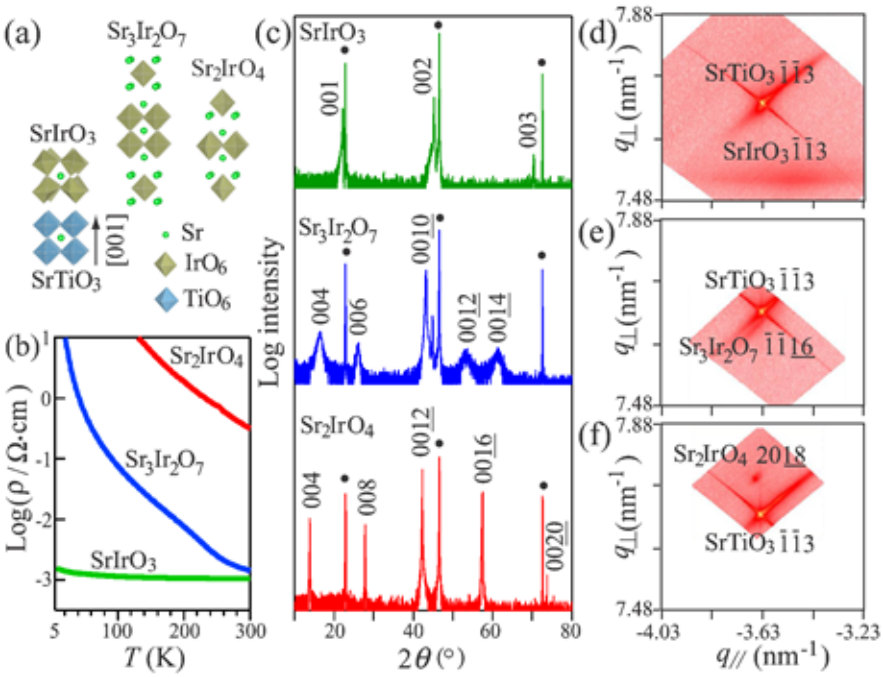

FIG. 1. (a) Crystal structures, (b) temperature dependent resistivity, and (c) out-of-plane XRD patterns of $SrIrO_3$, $Sr_3Ir_2O_7$, and Sr_2IrO_4 on a $SrTiO_3$ (001) substrate. Reciprocal space mapping for (d) pseudo-cubic $SrIrO_3$, (e) $Sr_3Ir_2O_7$, and (f) Sr_2IrO_4. Films were grown at P_{O2} = 100 mTorr, F = 3. 75 J·cm^{-2}, and at 600, 850, and 950 °C for $SrIrO_3$, $Sr_3Ir_2O_7$, and Sr_2IrO_4, respectively.

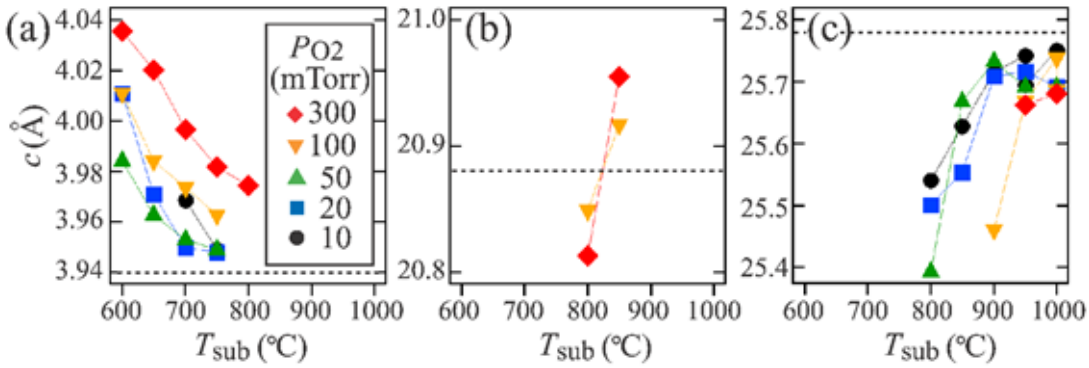

FIG. 2. *c*-axis lattice constants for films of (a) pseudo-cubic $SrIrO_3$, (b) $Sr_3Ir_2O_7$, and (c) Sr_2IrO_4 thin films, estimated from the out-of-plane XRD patterns. Films were grown under varied P_{O2} and T_{sub} at F = 3.75 J·cm^{-2}. Dashed lines are bulk reference values. [4,27,30]

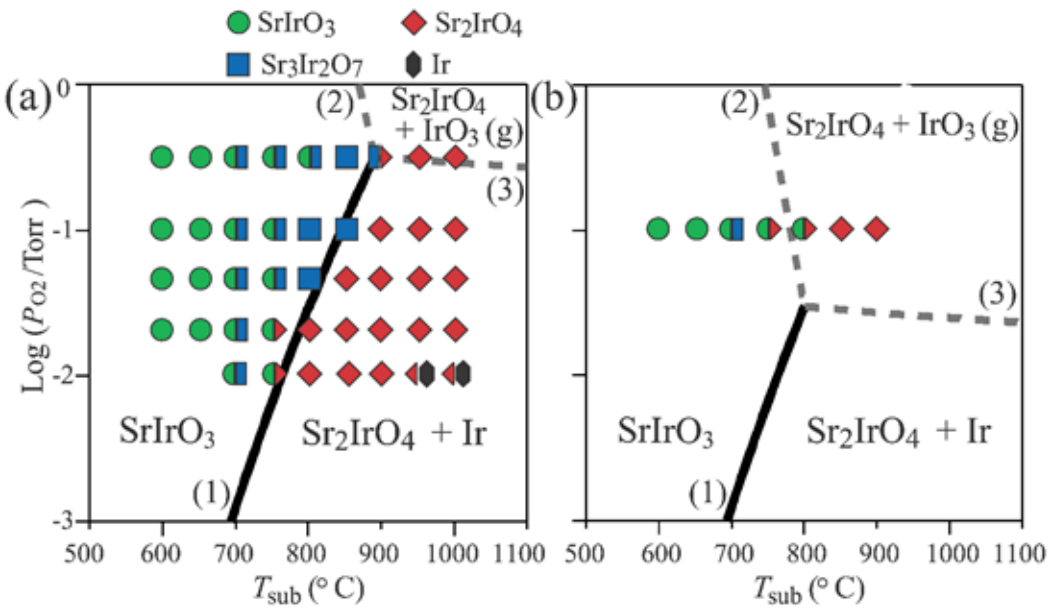

FIG. 3. Growth phase diagram for films grown at (a) F = 3.75 J·cm^{-2} and (b) F = 0.78 J·cm^{-2} with calculated phase boundaries according to Equations 1 (solid line), 2, and 3 (dotted lines). Partial pressure of IrO_3 (P_{IrO3}) is set to (a) 4 × 10^{-6} Torr and (b) 1 ×10^{-7} Torr. Composite symbols indicate mixed phases.

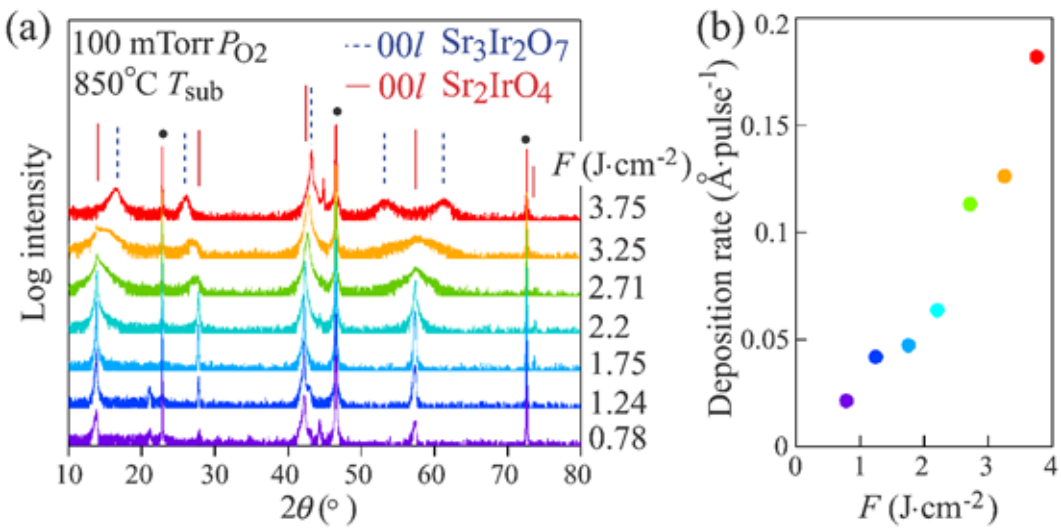

FIG. 4. (a) Out-of-plane XRD patterns for films grown at P_{O2} = 100 mTorr, and T_{sub} = 850 °C under varied F. (b) Ex-situ determined deposition rate dependence on F.

CONCLUSION: SUPPLEMENTARY MATERIAL

Information about depositing supplementary material may be found in Supporting Data in our Author Resource Center.

ACKNOWLEDGMENTS

This work is supported by the Department of Energy, Office of Basic Energy Sciences, Division of Materials Sciences and Engineering, and Laboratory Directed Research and Development funding (Y.H.), under contract DE-AC02-76SF00515.

REFERENCES

[a] knishio@stanford.edu

[1] K. Fujiwara, Y. Fukuma, J Matsuno, H. Idzuchi, Y. Niimi, Y. Ohtani, and H. Takagi, "5*d* Iridium Oxide as a Material for Spin-Current Detection." Nature Commun. **4**, 2893 (2013).

[2] K. A Modic, T. E. Smidt, I. Kimchi, N. P. Breznay, A. Biffin, S. Choi, R. D. Johnson, R. Coldea, P. Watkins-Curry, G. T. McCandless, J. Y. Chan, F. Gandara, Z. Islam, A. Vishwanath, A. Shekhter, R. D. McDonald, and J. G. Analytis, "Realization of a Three-Dimensional Spin-Anisotropic Harmonic Honeycomb Iridate." Nature Commun. **5**, 4203 (2014).

[3] D. Pesin, and L. Balents, "Mott Physics and Band Topology in Materials with Strong Spin-Orbit Interaction." Nature Phys. **6**, 376 (2010).

[4] J. G. Zhao, L. X. Yang, Y. Yu, F. Y. Li, R. C. Yu, Z. Fang, L. C. Chen, and C. Q. Jin, "High-Pressure Synthesis of Orthorhombic $SrIrO_3$ Perovskite and Its Positive Magnetoresistance." J. Appl. Phys. **103**, 103706 (2008).

[5] J. W. Kim, Y. Choi, J. Kim, J. F. Mitchell, G. Jackeli, M. Daghofer, J. van den Brink, G. Khaliulin, and B. J. Kim, "Dimensionality Driven Spin-Flop Transition in Layered Iridates." Phys. Rev. Lett. **109**, 037204 (2012).

[6] Y. Okada, D. Walkup, H. Lin, C. Dhital, T-R. Chang, S. Khadka, W. Zhou, H-T. Jeng, M. Paranjape, A. Bansil, Z. Wang, S. D. Wilson, and V. Madhavan, "Imaging the Evolution of Metallic States in a Correlated Iridate." Nature Mater. **12**, 707 (2013).

[7] S. Fujiyama, K. Ohashi, H. Ohsumi, K. Sugimoto, T. Takayama, T. Komesu, M. Takata, T. Arima, and H. Takagi, "Weak Antiferromagnetism of $J_{\mathrm{eff}} = 1/2$ Band in Bilayer Iridate $Sr_3Ir_2O_7$." Phys. Rev. B **86**, 174414 (2012).

[8] B. J. Kim, H. Jin, S. J. Moon, J-Y. Kim, B.-G. Park, C. S. Leem, J. Yu, T. W. Noh, C. Kim, S.-J. Oh, J.-H. Park, V. Durairaj, G. Cao, and E. Rotenberg, "Novel $J_{\mathrm{eff}} = 1/2$ Mott State Induced by Relativistic Spin-Orbit Coupling in Sr_2IrO_4." Phys. Rev. Lett. **101**, 076402 (2008).

[9] B. J. Kim, H. Ohsumi, T. Komesu,; S. Sakai, T. Morita, H. Takagi, and T. Arima, "Phase-Sensitive Observation of a Spin-Orbital Mott State in Sr_2IrO_4." Science **323**, 1329 (2009).

[10] J. Kim, M. Daghofer, A. H. Said, T. Gog, J. Van den Brink, G. Khaliullin, and B. J. Kim, "Excitonic Quasiparticles in a Spin-Orbit Mott Insulator." Nature Commun. **5**, 4453 (2014).

[11] S. J. Moon, H. Jin, K. W.Kim, W. S. Choi, Y. S. Lee, J. Yu, G. Cao, A. Sumi, H. Funakubo, C. Bernhard, and T. W. Noh,

"Dimensionality-Controlled Insulator-Metal Transition and Correlated Metallic State in 5*d* Transition Metal Oxides $Sr_{n+1}Ir_nO_{3n+1}$ ($n = 1, 2$, and ∞)." Phys. Rev. Lett. **101**, 226402 (2008).

[12] J. H. Gruenewald, J. Nichols, J. Terzic, G.Cao, J. W. Brill, and S. S. A. Seo, "Compressive Strain-Induced Metal-Insulator Transition in Orthorhombic $SrIrO_3$ Thin Films." J. Mater. Res. **29**, 2491 (2014).

[13] A. Biswas, K.-S. Kim, and Y. H. Jeong, "Metal Insulator Transitions in Perovskite $SrIrO_3$ Thin Films." J. Appl. Phys. **116**, 213704 (2014).

[14] J. Nichols, J. Terzic, E. G. Bittle, O. B. Korneta, L. E. De Long, J. W. Brill, G. Cao, and S. S. A. Seo, "Tuning Electronic Structure via Epitaxial Strain in Sr_2IrO_4 Thin Films." Appl. Phys. Lett. **102**, 141908 (2013).

[15] C. Lu, A. Quindeau, H. Deniz, D. Preziosi, D. Hesse, and M. Alexe, "Crossover of Conduction Mechanism in Sr_2IrO_4 Epitaxial Thin Films." Appl. Phys. Lett. **105**, 082407 (2014).

[16] C. R. Serrao, J. Liu, J. T. Heron, G. Singh-Bhalla, A. Yadov, S. J. Suresha, R. J. Paull, D. Yi, J.-H. Chu, M. Trassin, A. Vishwanath, E. Arenholz, C. Frontera, J. Železný, T. Jungwirth, X. Marti, and R. Ramesh, "Epitaxy-Distorted Spin-Orbit Mott Insulator in Sr_2IrO_4 Thin Films." Phys. Rev. B **87**, 085121 (2013).

[17] I. Barin, *Thermochemical Data of Pure Substances, 3rd ed.* (VCH, New York, 1995).

[18] T. Ohnishi, M. Lippma, T. Yamamoto, S. Meguro, and H. Koinuma, "Improved Stoichiometry and Misfit Control in Perovskite Thin Film Formation at a Critical Fluence by Pulsed Laser Deposition." Appl. Phys. Lett. **87**, 241919 (2005).

[19] J. H. Song, T. Susaki, and H. Y. Hwang, "Enhanced Thermodynamic Stability of Epitaxial Oxide Thin Films." Adv. Mater. **20**, 2528 (2008).

[20] H. K. Sato, C. Bell, Y. Hikita, and H. Y. Hwang, "Stoichiometry Control of the Electronic Properties of the $LaAlO_3/SrTiO_3$ Heterointerface." Appl. Phys. Lett. **102**, 251602 (2013).

[21] D. G. Schlom, Y. Jia, L.-N. Zou, J. H. Hanei, S. Briczinski, M. A. Zurbuchen, C. W. Leitz, M. Madhavan, S. Wozniak, Y. Liu, M. E. Hawley, G. W. Brown, A. Dabkowski, H. A. Dabkowska, R. Uecker, and P. Reiche, "Searching for Superconductivity in Epitaxial Films of Copper-Free Layered Oxides with the K_2NiF_4 Structure." *Proc. SPIE* **1998**, *3481*, 226.

[22] S. Ohashi, M. Lippmaa, N. Nakagawa, H. Nagasawa, H. Koinuma, and M. Kawasaki, "Compact Laser Molecular Beam Epitaxy System Using Laser Heating of Substrate for Oxide Film Growth." Rev. Sci. Instrum. **70**, 178 (1999).

[23] T. Ohnishi, and K. Takada, "Epitaxial Thin-Film Growth of $SrRuO_3$, $Sr_3Ru_2O_7$, and Sr_2RuO_4 from a $SrRuO_3$ Target by Pulsed Laser Deposition." Appl. Phys. Express **4**, 025501 (2011).

[24] T. Ohnishi, H. Koinuma, and M. Lippmaa, "Pulsed Laser Deposition of Oxide Thin Films." Appl. Surf. Sci. **252**, 2466 (2006).

[25] Y. K. Kim, A. Sumi, K. Takahashi, S. Yokoyama, S. Ito, T. Watanabe, K. Akiyama, S. Kaneko, K. Sato, and H. Funakubo, "Metalorganic Chemical Vapor Deposition of Epitaxial Perovskite $SrIrO_3$ Films on (100) $SrTiO_3$ Substrates." Jpn. J. Appl. Phys. **45**, L36 (2006).

[26] J. M. Longo, J. A. Kafalas, and R. J. Arnott, "Structure and Properties of the High and Low Pressure Forms of $SrIrO_3$." J. Solid State Chem. **3**, 174 (1971).

[27] M. A. Subramanian, M. K. Crawford, and R. L. Harlow, "Single Crystal Structure Determination of Double Layered Strontium Iridium Oxide [$Sr_3Ir_2O_7$]." Mater. Res. Bull. **29**, 645 (1994).

[28] H. Matsuhata,; I. Nagai, Y. Yoshida, S. Hara, S. Ikeda, and N. Shirakawa, "Crystal Structure of $Sr_3Ir_2O_7$ Investigated by Transmission Electron Microscopy." J. Solid State Chem. **177**, 3776 (2004).

[29] Q. Huang, J. L. Soubeyroux, O. Chmaissem, I. N. Sora, A. Santoro, R. J. Cava, J. J. Krajewski, and W. F. Peck, Jr., "Neutron Powder Diffraction Study of the Crystal Structures of Sr_2RuO_4 and Sr_2IrO_4 at Room Temperature and at 10K." J. Solid State Chem. **112**, 355 (1994).

[30] K. T. Jacob, T. H. Okabe, T. Uda, and Y. Waseda, "Phase Relations in the System Sr-Ir-O and Thermodynamic measurements on $SrIrO_3$, Sr_2IrO_4 and Sr_4IrO_6 using Solid-State Cells with Buffer Electrodes." J. Alloys. Compd. **288**, 188 (1999).

[31] D. B. Chrisey, and G. K. Hubler, *Pulsed Laser Deposition of Thin Films* (J. Wiley, New York, 1994).

[32] Y. F. Nie, Y. Zhu, C.-H. Lee, L. F. Kourkoutis, J. A. Mundy, J. Junquera, Ph. Ghosez, D. J. Baek, S. Sung, X. X. Xi, K. M. Shen, D. A. Muller, and D. G. Schlom, "Atomically Precise Interfaces from Non-Stoichiometric Deposition." Nature Commun. **5**, 4530 (2014).

[33] J. H. Lee, G. Luo, I. C. Tung, S. H. Chang, Z. Luo, M. Malshe, M. Gadre, A. Bhattacharya, S. M. Nakhmanson, J. A. Eastman, H. Hong, J. Jellinek, D. Morgan, D. D. Fong, and J. W. Freeland, "Dynamic Layer Rearrangement During Growth of Layered Oxide Films by Molecular Beam Epitaxy." Nature Mater. **13**, 879 (2014).